# Hybrid plasmonic-photonic modes in diffractive arrays of nanoparticles coupled to light-emitting optical waveguides

**S. Murai,[1,2,*] M. A. Verschuuren,[3] G. Lozano,[1] G. Pirruccio,[1] S. R. K. Rodriguez,[1] and J. Gómez Rivas[1,4]**

[1] *FOM Institute for Atomic and Molecular Physics AMOLF, c/o Philips Research Laboratories, High Tech Campus 4, 5656 AE, Eindhoven, The Netherlands*
[2] *Department of Material Chemistry, Graduate School of Engineering, Kyoto University, Katsura, Nishikyo-ku, Kyoto 615-8510, Japan*
[3] *Philips Research Laboratories, High Tech Campus 4, 5656 AE Eindhoven, The Netherlands*
[4] *COBRA Research Institute, Eindhoven University of Technology, P.O. Box 513, 5600 MB Eindhoven, The Netherlands*
[*] *murai@dipole7.kuic.kyoto-u.ac.jp*

**Abstract:** We study the hybridized plasmonic-photonic modes supported by two-dimensional arrays of metallic nanoparticles coupled to light-emitting optical waveguides. Localized surface plasmon polaritons in the metallic nanoparticles can couple to guided modes in the underlying waveguide, forming quasi-guided hybrid modes, or to diffracted orders in the plane of the array, forming surface lattice resonances. We consider three kinds of samples: one sustains quasi-guided modes only, another sustains surface lattice resonances only, and a third sample sustains both modes. This third sample constitutes the first demonstration of simultaneous coupling of localized surface plasmons to guided modes and diffracted orders. The dispersive properties of the modes in the samples are investigated through light extinction and emission spectroscopy. We elucidate the conditions that lead to the coexistence of surface lattice resonances and quasi-guided hybrid modes, and assess their potential for enhancing the luminescence of emitters embedded in the coupled waveguide. We find the largest increase in emission intensity for the surface lattice resonances, reaching up to a factor of 20.



**OCIS codes:** (240.6680) Surface plasmons; (050.1970) Diffractive optics; (230.7400) Waveguides, slab.

## References and links

1. A. V. Zayats and I. I. Smolyaninov, "Near-field photonics: surface plasmon polaritons and localized surface plasmons," J. Opt. A **5**, S16 (2003).
2. W. Murray and W. Barnes, "Plasmonic materials," Adv. Mater. **19**, 3771–3782 (2007).
3. E. Fort and S. Grsillon, "Surface enhanced fluorescence," J. Phys. D **41**, 013001 (2008).
4. P. Bharadwaj, B. Deutsch, and L. Novotny, "Optical antennas," Adv. Opt. Photon. **1**, 438–483 (2009).
5. J. A. Schuller, E. S. Barnard, W. Cai, Y. C. Jun, J. S. White, and M. L. Brongersma, "Plasmonics for extreme light concentration and manipulation," Nat. Mater. **9**, 193–204 (2010).

#179840 - $15.00 USD Received 19 Nov 2012; revised 28 Jan 2013; accepted 28 Jan 2013; published 12 Feb 2013

6. P. Zijlstra and M. Orrit, "Single metal nanoparticles: optical detection, spectroscopy and applications," Rep. Prog. Phys. **74**, 106401 (2011).
7. V. Giannini, A. I. Femandez-Dominiguez, S. C. Heck, and S. A. Maier, "Plasmonic Nanoantennas: Fundamentals and Their Use in Controlling the Radiative Properties of Nanoemitters," Chem. Rev. **111**, 3888–3912 (2011).
8. W. L. Barnes, "Fluorescence near interfaces: The role of photonic mode density," J. Mod. Opt. **45**, 661–699 (1998).
9. S. Kühn, U. Håkanson, L. Rogobete, and V. Sandoghdar, "Enhancement of single-molecule fluorescence using a gold nanoparticle as an optical nanoantenna," Phys. Rev. Lett. **97**, 017402 (2006).
10. P. Anger, P. Bharadwaj, and L. Novotny, "Enhancement and quenching of single-molecule fluorescence," Phys. Rev. lett. **96**, 113002 (2006).
11. O. L. Muskens, V. Giannini, J. A. Sánchez-Gil, and J. Gómez Rivas, "Strong enhancement of the radiative decay rate of emitters by single plasmonic nanoantennas," Nano Lett. **7**, 2871–2875 (2007).
12. R. M. Bakker, H.-K. Yuan, Z. Liu, V. P. Drachev, A. V. Kildishev, V. M. Shalaev, R. H. Pedersen, S. Gresillon, and A. Boltasseva, "Enhanced localized fluorescence in plasmonic nanoantennae," Appl. Phys. Lett. **92**, 043101 (2008).
13. P. Muhlschlegel, H.-J. Eisler, O. J. F. Martin, B. Hecht, and D. W. Pohl, "Resonant optical antennas," Science **308**, 1607–1609 (2005).
14. T. H. Taminiau, F. D. Stefani, F. B. Segerink, and N. F. van Hulst, "Optical antennas direct single-molecule emission," Nat. Photonics **2**, 234–237 (2008).
15. A. Kinkhabwala, Z. Yu, S. Fan, Y. Avlasevich, K. Mullen, and W. E. Moerner, "Large single-molecule fluorescence enhancements produced by a bowtie nanoantenna," Nat. Photonics **3**, 654–657 (2009).
16. T. Coenen, E. J. R. Vesseur, A. Polman, and A. F. Koenderink, "Directional emission from plasmonic yagiuda antennas probed by angle-resolved cathodoluminescence spectroscopy," Nano Lett. **11**, 3779–3784 (2011).
17. T. Kosako, Y. Kadoya, and H. F. Hoffman, "Directional control of light by a nano-optical Yagi-Uda antenna," Nat. Photonics **4**, 312–314 (2010).
18. S. Zou, N. Janel, and G. C. Schatz, "Silver nanoparticle array structures that produce remarkably narrow plasmon lineshapes," J. Chem. Phys. **120**, 10871–5 (2004).
19. V. G. Kravets, F. Schedin, and A. N. Grigorenko, "Extremely narrow plasmon resonances based on diffraction coupling of localized plasmons in arrays of metallic nanoparticles," Phys. Rev. Lett. **101**, 087403 (2008).
20. Y. Chu, E. Schonbrun, T. Yang, and K. B. Crozier, "Experimental observation of narrow surface plasmon resonances in gold nanoparticle arrays," Appl. Phys. Lett. **93**, 181108 (2008).
21. B. Auguié and W. L. Barnes, "Collective resonances in gold nanoparticle arrays," Phys. Rev. Lett. **101**, 143902 (2008).
22. W. Zhou and T. W. Odom, "Tunable subradiant lattice plasmons by out-of-plane dipolar interactions," Nat. Nanotech. **6**, 423–427 (2011).
23. A. Christ, S. G. Tikhodeev, N. A. Gippius, J. Kuhl, and H. Giessen, "Waveguide-Plasmon Polaritons : Strong Coupling of Photonic and Electronic Resonances in a Metallic Photonic Crystal Slab," Phys. Rev. Lett. **91**, 183901 (2003).
24. T. Zentgraf, S. Zhang, R. F. Oulton, and X. Zhang, "Ultranarrow coupling-induced transparency bands in hybrid plasmonic systems," Phys. Rev. B **80**, 195415 (2009).
25. S. R. K. Rodriguez, S. Murai, M. A. Verschuuren, and J. Gómez Rivas, "Light-emitting waveguide-plasmon polaritons," Phys. Rev. Lett. **109**, 166803 (2012).
26. F. J. García de Abajo and J. J. Sáenz, "Electromagnetic surface modes in structured perfect-conductor surfaces," Phys. Rev. Lett. **95**, 233901 (2005).
27. B. Auguié, X. M. Bendaña, W. L. Barnes, and F. J. García de Abajo, "Diffractive arrays of gold nanoparticles near an interface: Critical role of the substrate," Phys. Rev. B **82**, 155447 (2010).
28. V. A. Markel, "Divergence of dipole sums and the nature of non-lorentzian exponentially narrow resonances in one-dimensional periodic arrays of nanospheres," J. Phys. B **38**, L115–L121 (2005).
29. P. Schlotter, R. Schmidt, and J. Schneider, "Luminescence conversion of blue light emitting diodes," Appl. Phys. A **64**, 417–418 (1997).
30. M. A. Verschuuren and H. van Sprang, "3d photonic structures by sol-gel imprint lithography," in "Mater. Res. Soc. Sym. Proc.", (MRS, New York, NY, USA, 2007), N03–N05.
31. A. E. Gash, T. M. Tillotson, J. H. Satcher, J. F. Poco, L. W. Hrubesh, and R. L. Simpson, "Use of epoxides in the sol-gel synthesis of porous iron(III) oxide monoliths from Fe(III) salts," Chem. Mater. **13**, 999–1007 (2001).
32. S. Murai, K. Fujita, K. Iwata, and K. Tanaka, "Scattering-based hole burning in $Y_3Al_5O_{12}$: $Ce^{3+}$ monoliths with hierarchical porous structures prepared via the solgel route," J. Phys. Chem. C **115**, 17676–17681 (2011).
33. S. Murai, M. A. Verschuuren, G. Lozano, G. Pirruccio, A. F. Koenderink, and J. Gómez Rivas, "Enhanced absorption and emission of $Y_3Al_5O_{12}$: $Ce^{3+}$ thin layers prepared by epoxide-catalyzed sol-gel method," Opt. Mater. Express **2**, 1111–1120 (2012).
34. G. Vecchi, V. Giannini, and J. Gómez Rivas, "Surface modes in plasmonic crystals induced by diffractive coupling of nanoantennas," Phys. Rev. B **80**, 201401 (2009).
35. S. R. K. Rodriguez, A. Abass, B. Maes, O. T. A. Janssen, G. Vecchi, and J. Gómez Rivas, "Coupling bright and


#179840 - $15.00 USD Received 19 Nov 2012; revised 28 Jan 2013; accepted 28 Jan 2013; published 12 Feb 2013

dark plasmonic lattice resonances," Phys. Rev. X **1**, 021019 (2011).
36. S. A. Maier, *Plasmonics: Fundamentals and Applications*, 1st ed. (Springer, New York, 2007).
37. A. Christ, T. Zentgraf, J. Kuhl, S. G. Tikhodeev, N. A. Gippius, and H. Giessen, "Optical properties of planar metallic photonic crystal structures: experiment and theory," Phys. Rev. B **70**, 125113 (2004).
38. P. Yeh, *Optical Waves in Layered Media*, 1st ed. (Wiley-InterScience, College Station, Texas, 1998).
39. G. Vecchi, V. Giannini, and J. Gómez Rivas, "Shaping the fluorescent emission by lattice resonances in plasmonic crystals of nanoantennas," Phys. Rev. Lett. **102**, 146807 (2009).
40. V. Giannini, G. Vecchi, and J. Gómez Rivas, "Lighting up multipolar surface plasmon polaritons by collective resonances in arrays of nanoantennas," Phys. Rev. Lett. **105**, 266801 (2010).
41. G. Pellegrini, G. Mattei, and P. Mazzoldi, "Nanoantenna arrays for large-area emission enhancement," J. Phys. Chem. C **115**, 24662–24665 (2011).
42. S. R. K. Rodriguez, G. Lozano, M. A. Verschuuren, R. Gomes, K. Lambert, B. D. Geyter, A. Hassinen, D. V. Thourhout, Z. Hens, and J. Gómez Rivas, "Quantum rod emission coupled to plasmonic lattice resonances: A collective directional source of polarized light," Appl. Phys. Lett. **100**, 111103 (2012).
43. W.-H. Chao, R.-J. Wu, C.-S. Tsai, and T.-B. Wu, "Surface plasmon-enhanced emission from Ag-coated Ce doped $Y_3Al_5O_{12}$ thin films phosphor capped with a dielectric layer of $SiO_2$," J. Appl. Phys. **107**, 013101 (2010).
44. FDTD Solutions, from Lumerical Solutions Inc., http://www.lumerical.com/.
45. P. B. Johnson and R. W. Christy, "Optical constants of the noble metals," Phys. Rev. B **6**, 4370–4379 (1972).
46. H. A. Atwater and A. Polman, "Plasmonics for improved photovoltaic devices," Nat. Mater. **9**, 205–213 (2010).
47. P. Offermans, M. C. Schaafsma, S. R. K. Rodriguez, Y. Zhang, M. Crego-Calama, S. H. Brongersma, and J. Gómez Rivas, "Universal scaling of the figure of merit of plasmonic sensors," ACS Nano **5**, 5151–5157 (2011).

## 1. Introduction

Plasmonic nanostructures are currently being intensively investigated. The reason for this pronounced interest is their very large polarizability due to localized surface plasmon resonances (LSPRs), which allows to enhance light-matter interactions [1–7]. LSPRs are the coherent oscillation of the free electrons in metallic nanoparticles driven by an external electromagnetic field. If an optical emitter is located in the proximity of a metallic particle, it can decay by exciting LSPRs. The emitter experiences a modified local density of optical states (LDOS) due to the presence of the nanoparticle, which influences its radiative and non-radiative decay rates [8–12]. LSPRs can also radiate into the far field by coupling to radiation modes in the medium surrounding the particles. Metallic particles supporting plasmonic resonances are, thus, capable of modifying the emission of nanosources. This important characteristic has led to the term optical antenna or nanoantenna when referring to metallic nanoparticles in analogy to radio-wave antennas [13]. Several types of optical antennas have been reported, e.g., single nanoparticles [9, 10], nanorods [13, 14], dimer and bowtie antennas [11, 15], Yagi-Uda antennas [16, 17], and arrays of nanoparticles [18–22].

While single metallic nanoparticles can sustain LSPRs, a periodic array of these nanostructures may exhibit collective resonances resulting from the radiative coupling of LSPRs. Of particular interest are periodic arrays of metallic nanoparticles with a lattice constant comparable to the wavelength of light. In these arrays, the radiative coupling can be enhanced by surface or guided modes. Two distinct mechanisms enhancing the radiative coupling of LSPRs have been reported in literature. The first one consists of the hybridization of guided modes in thin dielectric layers with LSPRs of nanoparticles in the proximity of the guiding layer [23–25]. For these hybridized modes, which we will refer to as quasi-guided modes, a waveguiding structure is necessary. The second mechanism relies on Rayleigh anomalies (RAs) or diffracted orders in the plane of the array, which lead to the hybridized resonances known as surface lattice resonances (SLRs) [26]. SLRs are favored when the array of nanoparticles is embedded in an homogeneous dielectric [27] and for large nanoparticles [27, 28]. Although both quasi-guided modes and SLRs have been extensively studied, they have never simultaneously reported in a single sample because of the different conditions to support them: Quasi-guided modes need a waveguide that has a higher refractive index than the surrounding, while SLRs are favored when the medium surrounding the array is homogeneous.

#179840 - $15.00 USD Received 19 Nov 2012; revised 28 Jan 2013; accepted 28 Jan 2013; published 12 Feb 2013

In this article, we study the conditions that allow the excitation of quasi-guided modes and SLRs to achieve the coexistence of both modes in single structures. In order to identify and compare both modes, we fabricate plasmonic arrays on top of a thin layer of emitting material acting as a light-emitting waveguide, and examine them through light extinction and emission spectroscopy. In particular, we demonstrate for the first time the simultaneous observation of both modes by minimizing the mismatch in refractive index between the media surrounding the plasmonic array. We explore the coupling of these modes with the optical emitters located in the waveguide through the measurement of the photoluminescence spectra. A strong modification of the luminescence as a result of the coupling is noticed, showing that the emission from the coupled waveguide is a powerful probe to investigate the optical density of states associated with the hybrid modes.

The article is organized as follows. In section 2 we describe the preparation of three different sample configurations: One supporting SLRs, the second supporting quasi-guided modes and the third supporting both types of resonances. The extinction properties of those samples are elucidated in section 3. In section 4, we examine the emission enhancement of the optical emitters in the waveguide coupled to these plasmonic-photonic modes. We observe a far-field photoluminescence which is modified both spectrally and spatially. In section 5, we examine the spatial distribution of the SLRs, quasi-guided modes, and LSPRs by using a 3D finite-difference time-domain (FDTD) simulation.

## 2. Sample preparation

We have prepared three samples in order to identify the different resonances in periodic arrays of plasmonic antennas. The first sample consists of an array of Ag nanorods homogenously surrounded by sapphire ($Al_2O_3$). Figure 1 shows a scanning electron microscope image of a top view of the antenna array. The second one is a similar array of Ag nanorods inhomogeneously surrounded by a waveguide layer on a $SiO_2$ substrate on one side and air on the other side. As a waveguide, $Ce^{3+}$ doped yttrium aluminium garnet (YAG:Ce) was selected because of its higher refractive index compared to $SiO_2$. YAG:Ce is also known as an important luminescent material currently used in white light-emitting diodes(W-LEDs) [29]. Its broad emission in the visible centered at 580 nm is useful to study its coupling to the dispersive plasmonic-photonic modes in a wide spectral range. The third sample represents an intermediate case, with a similar array of nanorods with a waveguide layer on top of $SiO_2$, and a $SiO_2$ upperstrate on the other side. A schematic representation of the samples can be found in the inset of Figs. 2(a), (b) and (c). In the following we describe the preparation of these three samples.

The first sample was prepared on an $Al_2O_3$ substrate. An array of Ag nanorods was fabricated on the substrate by using substrate conformal imprint lithography (SCIL) [30]. The array consisted of rectangular rods of 20 nm height with long (short) axis of 300 nm (70 nm) along the x (y) direction arranged in a lattice with constants $a_x$ = 500 nm and $a_y$ = 200 nm. An upperstrate of $Al_2O_3$ was optically matched to the substrate with a refractive index matching liquid [not shown in the inset of Fig. 2(a)].

The YAG:Ce waveguides of the second and third samples were fabricated on $SiO_2$ glass substrates via a sol-gel route by using propylene oxide as a gelation initiator [31,32]. A detailed description of the synthesis of similar layers can be found in Ref. [33]. First, a YAG layer (thickness $\leq$ 50 nm) was deposited as a buffer layer, and a YAG:Ce layer was deposited on top. The total thickness of the two layers(YAG + YAG:Ce) was 230 $\pm$ 30 nm. The nominal composition of the YAG:Ce film was $(Y_{0.95}Ce_{0.05})_3Al_5O_{12}$, i.e, 5mol% of $Y^{3+}$ was replaced by $Ce^{3+}$. The film was heated at 1000 °C in air for 1 h, and then 1000 °C in $H_2/N_2$ gas for another hour. The buffer layer avoids the reaction between YAG:Ce and $SiO_2$ during the heat treatment. After the deposition of a 20 nm thick layer of $Si_3N_4$ for planarization, a similar

#179840 - $15.00 USD Received 19 Nov 2012; revised 28 Jan 2013; accepted 28 Jan 2013; published 12 Feb 2013

nanorod array to that of the first sample was made using SCIL. In the third sample we used a $SiO_2$ upperstrate in optical contact with the nanorod array by means of a refractive index matching layer [not shown in the inset of Fig. 2(c)].

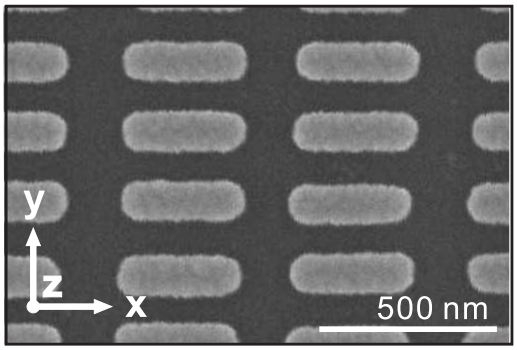


Fig. 1. Scanning electron microscope top view image of an Ag nanorod array.

## 3. Extinction measurements

The optical extinction of the three different arrays was determined by measuring the zeroth-order transmittance as a function of the angle of incidence. For these measurements we used the collimated beam from a halogen lamp with a beam diameter of $\simeq 0.5$ mm. The samples were mounted on a computer controlled rotation stage. The polarization of the incident light was set along the y axis, probing the short axis of the nanorods. The wave vector component of the incident plane wave parallel to the surface along the x axis was varied by rotating the sample to change the angle of incidence on the array in the x-z plane. The absolute zeroth-order transmittance ($T$) was obtained by normalizing the transmission of the incident light through the samples to that of the same samples but without the array of nanorods. The extinction is defined as $1-T$.

Figure 2 summarizes one of the main results of this article, namely, it presents a comparison of the extinction of the three arrays. Figure 2(a) shows the extinction of the first array consisting of Ag nanorods homogenously surrounded by $Al_2O_3$. The top panel plots the extinction in a color scale as a function of the wavelength $\lambda$ and the angle of incidence $\theta_{\text{inc}}$ of the beam with respect to the normal to the surface. In order to examine the dispersion of the extinction in detail, we have represented in the bottom panel the data as a function of the photon energy, $E = hc/\lambda$, and the in-plane wave vector of the incident beam, i.e., the projection of the incident wave vector onto the surface of the array, $k_{\text{inc}_{||}} = \frac{2\pi}{\lambda}\sin(\theta_{\text{inc}})$, with $c$ the speed of light. The solid lines in this figure indicate the RAs of the nanorod array or the onset of diffraction, i.e., the frequencies and angles of incidence at which a diffracted order is grazing to the plane of the array. These RAs correspond to the $(m_1, m_2)$=$(\pm 1, 0)$ diffracted orders. When $k_{\text{inc}_{||}}$ does not have a component in the y direction, the RAs satisfy the relation $k^2_{\text{out}} = k^2_{\text{inc}_{||}} + m_1^2(2\pi/a_x)^2 + m_2^2(2\pi/a_y)^2 + 2k_{\text{inc}_{||}} m_1(2\pi/a_x)$, where $k_{\text{out}}$ is the wave vector of the scattered light by the array. These RAs are calculated using the refractive index of 1.74 for an homogeneous medium surrounding the array of nanorods, which corresponds to the refractive index of $Al_2O_3$ in the visible. A broad and non dispersive extinction band is observed around $E = 2.1$ eV ($\lambda = 580$ nm), which corresponds to the excitation of the LSPRs in the Ag nanorods. In addition, we also see two extinction bands which follow the dispersion of the RAs. These bands correspond to the SLRs, which arise from the coupling of the LSPRs with the

#179840 - $15.00 USD Received 19 Nov 2012; revised 28 Jan 2013; accepted 28 Jan 2013; published 12 Feb 2013

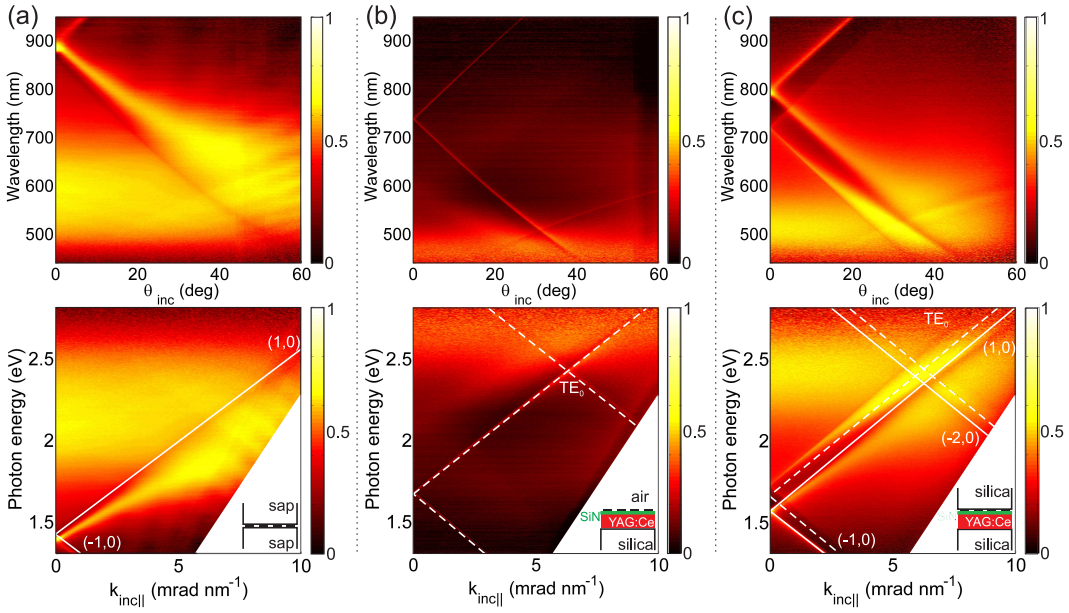


Fig. 2. Extinction measurements of arrays of Ag nanorods in different environments as a function of the wavelength and the angle of incidence $\theta_{\text{inc}}$ (top panels). The extinction is defined as $1-T$ where $T$ is the zeroth-order transmittance. The same measurements are represented in the bottom panels as a function of the photon energy and the in-plane wave vector of the incident light, $k_{\text{inc}_{||}}$. (a) corresponds to an array fabricated on an $Al_2O_3$ substrate and covered by an $Al_2O_3$ upperstrate. (b) is the measurements of a similar array on a $Si_3N_4$-planarized YAG:Ce layer fabricated on a $SiO_2$ glass substrate. (c) corresponds to the measurements of a similar array on a $Si_3N_4$-planarized YAG:Ce layer on a $SiO_2$ glass substrate, covered by a $SiO_2$ upperstrate. The incident light is polarized along the y direction, i.e., parallel to the short axis of the nanorods. In the bottom panels, the Rayleigh anomalies and the dispersion of the fundamental $TE_0$ mode guided in the YAG:Ce layer are also plotted. The insets in the bottom panels show a schematic illustration of the samples.

RAs forming the hybrid photonic-plasmonic mode. Because of this coupling with the LSPRs, the SLRs do not exactly coincide with the RAs but they are slightly red-shifted. The coupling strength between the RAs and the LSPRs increases as the frequency difference between them decreases, i.e., for larger values of $\theta_{\text{inc}}$ or $k_{\text{inc}_{||}}$. This increased coupling also leads to larger red-shift of the SLR and a broadening of the extinction, which indicate that the characteristics of the SLR approach to those of the LSPR. [34, 35].

Figure 2(b) shows the extinction measurements of the array of Ag nanorods on top of the YAG:Ce layer. For this sample the LSPR is at $E = 2.6$ eV or $\lambda = 470$ nm, i.e., it is blue shifted compared to the array embedded in $Al_2O_3$. This blue shift is the result of the lower index of refraction of the media surrounding the nanorods, which reduces the depolarization field, increasing the resonance energy [36]. We also see three dispersive and sharp resonances. The narrow width of these resonances indicates their high quality factors. The excitation of SLRs is favored when the array of nanorods is embedded in an homogeneous medium with the same index of refraction on both sides of the array [27]. Given that the sample used in Fig. 2(b) is very asymmetric in terms of the refractive index, the sharp resonances are not attributed to SLRs. Instead, these resonances correspond to the fundamental $TE_0$ guided mode in the YAG:Ce layer coupled to the LSPRs of the nanorods. The YAG:Ce layer acts as a slab waveguide due to its

#179840 - $15.00 USD Received 19 Nov 2012; revised 28 Jan 2013; accepted 28 Jan 2013; published 12 Feb 2013

high refractive index compared to the $SiO_2$ substrate and air. Here the antenna array plays the role of a grating that scatters the incident light into the guided mode or couples the guided mode into free space radiation. As a result, this mode becomes leaky [23, 24, 37].

The dispersion relation of the $TE_0$ guided mode calculated for a three layer system without an antenna array is plotted in the bottom panel of Fig. 2(b) [38]. In this calculation, we consider a YAG:Ce waveguide with a thickness of 200 nm and a refractive index $n = 1.67$, sandwiched in between an upper and lower medium of infinite thickness and a refractive index of $SiO_2$ glass (1.46) and air (1.0). The value of $n$ of the YAG:Ce layer used for these calculations is very similar to the value obtained from the ellipsometry measurements ($n = 1.68$ at $\lambda = 700$ nm). The dispersion is folded into the first Brillouin zone of the periodic array by taking into account the pitch in the x direction ($a_x$ = 500 nm). The edge of the first Brillouin zone ($\pi/a_x$) is at the wave number = 6.28 mrad $nm^{-1}$. The calculated dispersion of the $TE_0$ modes follows very well the measured extinction features, indicating their weaker hybridization with LSPRs compared to the SLRs in Fig. 2(a), which shows a large redshift and a broadening.

Figure 2(c) displays the extinction of the Ag nanorods array on top of the YAG:Ce waveguide with a $SiO_2$ upperstrate. The upperstrate increases the refractive index of the upper medium, reducing the index mismatch with the lower medium and allowing the excitation of SLRs. Consequently, both the SLRs and the quasi-guided modes can be observed in this sample. At normal incidence, the SLR is observed at $E = 1.56$ eV or $\lambda = 793$ nm, while the quasi-guided mode appears at a higher frequency ($E = 1.72$ eV) or a shorter wavelength ($\lambda = 722$ nm). We also plot in the bottom panel the RAs and the dispersion of the $TE_0$ mode. Here, the Rayleigh anomaly is calculated using an effective index of refraction of 1.58. Since the array is surrounded by several materials, i.e., $SiO_2$ glass ($n$ =1.46), $Si_3N_4$ ($n$ =2.0) and YAG:Ce ($n$ =1.68), this effective index is an averaged refractive index weighted by the spatial distribution of the mode. The $TE_0$ mode is calculated with the same parameters used in Fig. 2(b) except for the refractive index of the upper layer, which is increased from 1.0 to 1.43, and that of the YAG:Ce, which is reduced from 1.67 to 1.63. We need to slightly modify the refractive index of the YAG:Ce layer to fit to the extinction, probably because of the coupled nature of these modes with the nanorod array, which induces a shift with respect to the dispersion of the uncoupled waveguide.

## 4. Photoluminescence enhancement measurements

It has been recently proposed and demonstrated that SLRs lead to an enhanced and modified emission of sources in the proximity of the array of nanoparticles [39–42]. In this section we demonstrate the modified emission of the YAG:Ce layer simultaneously coupled to quasi-guided modes and SLRs. Recently, an enhancement of the emission from a YAG:Ce layer, mediated by Ag islands randomly deposited on top of the layer, was reported [43]. However, no modified emission spectrum or directionality were achieved. Our sample is similar to the one used in Fig. 2(b), except that the array is covered by a conformal layer of $Si_3N_4$ with a thickness of 20 nm to protect the Ag nanorods from oxidation [see a schematic illustration of the sample in Fig. 3(a)]. The $Si_3N_4$ layer also increases the effective index of refraction of the upper medium, providing a more symmetric surrounding to the nanorod array. As we have seen in the previous section, this symmetry is crucial for the excitation of SLRs.

Photoluminescence measurements were performed by illuminating the sample from the front side (the side with an antenna array) with a diode laser ($\lambda = 442$ nm, polarization parallel to the x axis) at an angle of $10^\circ$ from the normal to the sample. The emission polarized along the short axis of the nanorods was collected from the backside of the sample by a fiber coupled spectrometer mounted on a computer controlled rotation arm, which could be rotated in the x-z plane around the excitation spot.

In Fig. 3, we compare the extinction and photoluminescence measurements of the sample.

#179840 - $15.00 USD Received 19 Nov 2012; revised 28 Jan 2013; accepted 28 Jan 2013; published 12 Feb 2013

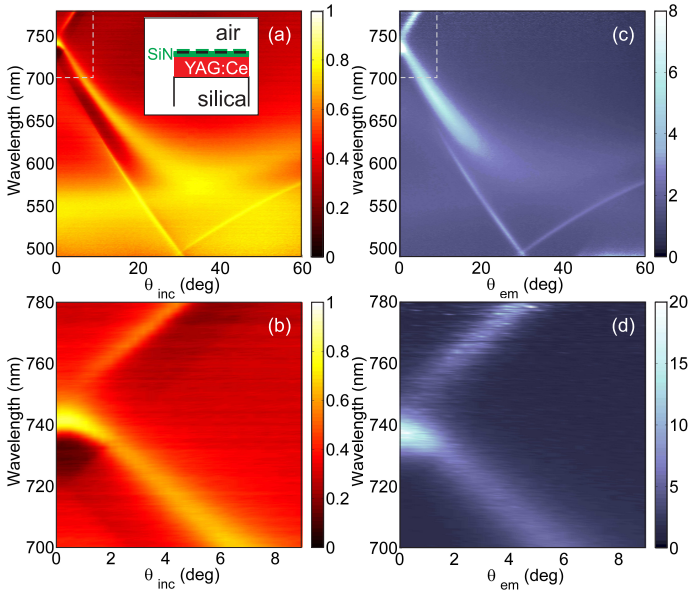


Fig. 3. (a) Extinction (color scale), plotted as a function of the wavelength and the angle of incidence $\theta_{inc}$, of an Ag nanorod array fabricated on a $Si_3N_4$-planarized YAG:Ce layer on a $SiO_2$ glass substrate and covered by a 20 nm passivation layer of $Si_3N_4$. The incident light is polarized along the y direction, i.e., parallel to the short axis of the nanorods, and the extinction is defined as 1-$T$ where $T$ is the zeroth-order transmittance. The inset shows a schematic illustration of the sample. (b) Magnified image of the area indicated by the dashed square in (a). (c) Photoluminescence enhancement defined as the fluorescent intensity of the sample normalized by the intensity of a similar YAG:Ce layer without antenna array on top, plotted as a function of the wavelength and the angle of emission with respect to the normal to the surface, $\theta_{em}$. We collected the light polarized along the y direction. Note that the photoluminescent enhancement is saturated to a value of 8 in this plot. (d) Magnified image of the area indicated by the dashed square in (c).

Figure 3(a) shows the zeroth-order extinction spectrum of the array plotted as a function of the wavelength and the angle of incidence $\theta_{inc}$. Sharp bands of high extinction are visible across the broad extinction band of the LSPR centered around $\lambda = 550$ nm, which are due to the excitation of quasi-guided modes in the YAG:Ce layer. In addition, SLRs appear at longer wavelengths than the LSPRs. The SLRs are located at $\lambda = 742$ nm for normal incidence, with one resonance assigned to the (-1, 0) RA and shifting to longer wavelengths, and the other assigned to the (+1, 0) RA and shifting to shorter wavelengths with increasing $\theta_{inc}$. In the magnified view of the extinction for small angles [Fig. 3(b)], the dispersion of the (+1, 0) SLR flattens and the extinction increases at normal incidence. In contrast, the extinction of the (-1, 0) SLR is reduced at small angles. This behavior is explained in terms of the coupling between the two degenerated SLRs at normal incidence [35]. The same behavior has also been observed for the degenerated quasi-guided modes [23].

In Figs. 3(c) and 3(d), we plot the photoluminescence (PL) enhancement of the sample, i.e., the emission spectra normalized by the emission of a reference YAG:Ce layer without the nanorod array on top, as a function of the wavelength and the angle of the emission from the normal to the surface, $\theta_{em}$. The PL enhancement follows the dispersion of the extinction shown in Figs. 3(a) and 3(b), i.e., relative maxima in the enhancement are achieved at the wavelengths

#179840 - $15.00 USD Received 19 Nov 2012; revised 28 Jan 2013; accepted 28 Jan 2013; published 12 Feb 2013

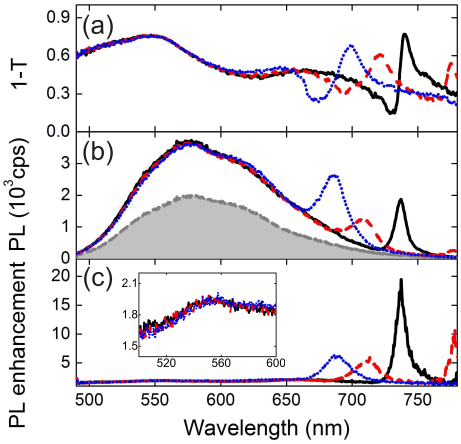


Fig. 4. (a) Cuts to the extinction measurements ($1-T$) of Fig. 3(a) at angles of incidence $\theta_{inc}$ = 0° (black solid curve), 4° (red dashed curve), and 7° (blue dotted curve). (b) Photoluminescence (PL) spectra at detection angles $\theta_{em}$ = 0°, 4°, and 7° (solid, dashed and dotted curves, respectively) . The gray filled area corresponds to the emission spectrum of a YAG:Ce layer without the array at $\theta_{em}$ = 0°. (c) PL enhancement at the same angles. The inset shows the magnified plot from 500 nm to 600 nm.

and angles of the SLRs, the quasi-guided modes, and in a lesser extent of the LSPRs. Among these maxima, the most pronounced corresponds to that of the SLR with a 20-fold enhancement at normal incidence at 737 nm [see Fig. 3(d), note that the scale is different from that in 3(c)], where the flattening of the mode is observed. The enhancement of the emission can be described in terms of three different contributions at the frequency of excitation and emission. At the frequency of excitation, the local enhancement of the electromagnetic field at resonant frequencies can lead to an increased absorption by the YAG:Ce and the concomitant increase of the emission. In our experiments, the contribution of the excitation frequency to the PL enhancement is negligible, since the antenna array is not resonant at the frequency and angle of incidence of the excitation beam. The other two contributions to the emission enhancement are at the frequency of emission; one corresponds to the increase of the LDOS to which the emitter can decay radiatively; and the other is the increased efficiency of the light extraction from the structure into free space.

It is also noticed in Fig. 3 that the relative magnitude of the PL enhancement does not agree with the magnitude of extinction. For example, the PL enhancement associated to the LSPRs is less pronounced compared to the others, although the extinction due to the LSPRs is very large. The relation between extinction and emission is further examined in Fig. 4, which presents the (a) $1-T$, (b) PL spectra, and (c) PL enhancement, obtained at different angles. In Fig. 4(a), we plot extinction at the incident angles $\theta_{inc}$ = 0° (solid curve), 4°(dashed curve), and 7° (dotted curve). For all the angles, one can see a broad resonance centered at 550 nm, which is due to the excitation of LSPRs in the individual rods. We also see the (+1, 0) SLR at a longer wavelength with an asymmetric, Fano-like, line shape. This resonance blue shifts as the angle increases. For the spectrum at $\theta_{inc}$ = 4°, we also see a resonance at 776 nm, which corresponds to the (-1, 0) SLR. Figure 4(b) displays the PL spectra collected at $\theta_{em}$ = 0°(solid curve), 4°(dashed curve), and 7° (dotted curve). The spectrum of a reference YAG:Ce layer without the antenna array at $\theta_{em}$ = 0° is also plotted as a filled area, showing the typical broadband emission of

#179840 - $15.00 USD Received 19 Nov 2012; revised 28 Jan 2013; accepted 28 Jan 2013; published 12 Feb 2013

YAG:Ce peaking at 575 nm. The emission from the YAG:Ce layer in the proximity of the array is more intense compared to the reference, besides the additional PL enhancement at the resonances. Figure 4(c) displays the PL enhancement collected at $\theta_{em}$ = 0° (solid curve), 4°(dashed curve), and 7° (dotted curve). The inset shows the magnified image at the wavelengths of the LSPRs. The PL enhancement factor at these wavelengths is around 2, which is up to an order of magnitude smaller compared to that of the SLR.

The extinction maps in Figs. 3(a) and 3(b) give information on the dispersion of the optical modes that can couple to far-field electromagnetic waves. However, they do not tell anything about the spatial distribution of the fields associated to these modes in the sample. Thus the discrepancy in extinction and PL enhancement can be related to the difference in the spatial distribution between a mode relative to the emitting YAG:Ce layer, which affects the LDOS and the outcoupling efficiency. In case of the LSPRs for example, the PL enhancement is small because of the strongly localized nature of these resonances, which leads to a modification of the LDOS only very close to the metallic nanorods while the emitters are located below the array separated by a 20 nm of $Si_3N_4$. In contrast, a large PL enhancement along the SLR and quasi-guided modes suggests a large spatial overlap between these modes and the layer of emitters. It is important to notice that the magnitude of enhancement varies even within a single SLR. In Fig. 3(c), the largest enhancement is seen at normal incidence along the (+1, 0) SLR, while it is less notable as the wavelength of SLR approaches that of LSPRs. At normal incidence, the flattened dispersion in extinction means a standing-wave nature of this mode, which provides a large density of states at this wavelength.

Figure 5(a) shows the extinction of the sample similar to the one used in Fig. 3 but with a $SiO_2$ upperstrate on the top [see a schematic illustration in Fig. 5(a)]. It is clearly seen that at normal incidence($\theta_{inc} = 0\ ^\circ$), both the SLR ($\lambda = 810$ nm) and the quasi-guided mode ($\lambda = 719$ nm) are excited. The wavelengths of the SLR and the quasi-guided mode are similar to those in Fig. 2(c), while the extinction is larger. This larger extinction is due to the stronger hybridization of these modes with the LSPRs, i.e., since Ag nanorods are coated by $Si_3N_4$ and surrounded by $SiO_2$, the frequency of the LSPRs is red-shifted increasing its coupling with the RAs and quasi-guided modes. The flattening of the SLR and quasi-guided mode is observed at $\theta_{inc} = 0\ ^\circ$. Moreover, the interaction between the SLR and quasi-guided mode is seen when they cross at $\theta_{inc} = 6.5\ ^\circ$ and $\lambda = 770$ nm. This indicates that both modes spatially overlap. The PL enhancement of the same sample is shown in Fig. 5(b). The enhancement follows the extinction features of SLRs and quasi-guided modes. The correspondence is better described in Fig. 5(c), which compares 1 - $T$ at $\theta_{inc} = 0\ ^\circ$ and PL enhancement at $\theta_{em} = 0\ ^\circ$. The extinction spectrum shows three extinction peaks, assigned to the LSPRs ($\lambda = 560$ nm), the quasi-guided mode ($\lambda = 719$ nm), and the SLR ($\lambda = 810$ nm). In the PL enhancement spectrum, three peaks associated with these modes are observed, and the largest enhancement is obtained for the SLR.

## 5. Numerical simulation

In order to explore the spatial distribution of the SLRs, the quasi-guided modes, and the LSPRs, we have conducted 3D FDTD simulations using a commercial package [44]. The unit cell of the simulated structure is shown in Fig. 6(a). The structure is similar to the sample in Fig. 5, where the $SiO_2$ upperstrate is placed on the Ag nanorod array to homogenize the refractive index around the array. The top panel shows the top view of the structure. The size of the nanorod is 300 (in x direction) $\times$ 70 (y)$\times$ 20 (z) $nm^3$. Periodic boundary conditions are applied in the lateral directions to simulate the array, i.e., a period of 500 (200) nm in x (y) direction. The bottom panel shows the cross section of the structure, consisting of a $SiO_2$ glass substrate, a YAG:Ce layer, a $Si_3N_4$ layer 20 nm thick, a Ag nanorod, another 20 nm conformal layer of $Si_3N_4$, and a $SiO_2$ glass upperstrate on the top. A single layer of YAG:Ce was used in the sim-

#179840 - $15.00 USD Received 19 Nov 2012; revised 28 Jan 2013; accepted 28 Jan 2013; published 12 Feb 2013

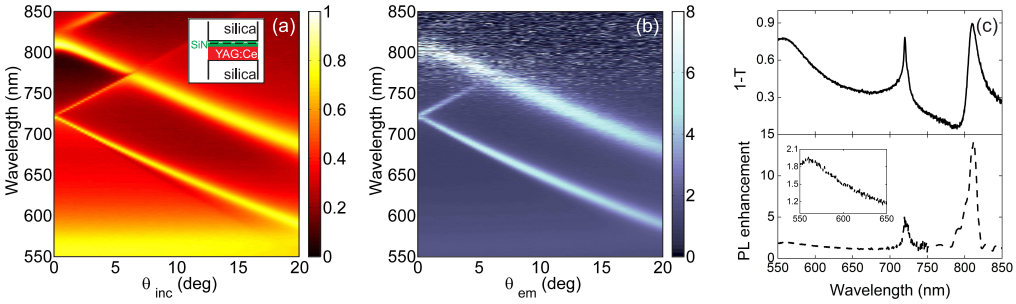


Fig. 5. (a) Extinction (color scale), plotted as a function of the wavelength $\lambda$ and the angle of incidence $\theta_{\mathrm{inc}}$, of a similar Ag nanorod array that employed in Fig. 3, but with a $SiO_2$ glass upperstrate on the top. The inset shows a schematic illustration of the sample. The incident light is polarized along the y direction, i.e., parallel to the short axis of the nanorods. (b) Photoluminescence enhancement of light polarized along the y direction as a function of $\lambda$ and the angle of emission with respect to the normal to the surface, $\theta_{\mathrm{em}}$. (c) 1 - $T$ at $\theta_{\mathrm{inc}} = 0\,^{\circ}$ (top panel) and PL enhancement at $\theta_{\mathrm{em}} = 0\,^{\circ}$ (bottom). The inset shows the magnified plot from $\lambda = 550$ to 650 nm. PL enhancement above $\lambda = 750$ nm is smoothed by adjacent averaging over a 10 nm window because the emission intensity of YAG:Ce is weak in this spectral region.

ulation instead of the stack of the YAG buffer layer and the YAG:Ce layer. This simplification is justified because the permittivity of YAG is similar to that of YAG:Ce. The thickness of the YAG:Ce layer, $d$, was varied as 200, 250, and 300 nm. We have used a constant refractive index of 1.46 for $SiO_2$ glass, 1.69 for YAG:Ce, and 2.0 for $Si_3N_4$, and the dispersive permittivity of Ag was taken from Ref. [45]. The incident light was linearly-polarized with the electric field parallel to the y direction or the short axis of the nanorod.

Figure 6(b) displays the simulated extinction, $1 - T$, in which $T$ is calculated as the transmitted power through the structure normalized to the input power. When $d$ = 200 nm (denoted by black solid curve), a broad peak at $\lambda = 650$ nm and a sharp peak at 804 nm are observed, with a small bump at 730 nm. The broad peak corresponds to the excitation of LSPRs while the features observed at longer wavelengths correspond to the (+1, 0) SLR and the quasi-guided mode, respectively. Although the spectral position of the LSPR is red-shifted and the extinction of the quasi-guided mode is much weaker compared to the experimental data in Fig. 5(c), all the spectral features are qualitatively reproduced. As the thickness $d$ increases, the quasi-guided mode displayed at $\lambda = 730$ nm grows in extinction and the spectral position of the SLR at 804 nm is red-shifted. The increase in extinction of the guided mode indicates that the coupling of the incident light to the guided mode becomes more efficient by increasing the thickness of the waveguide. The redshift of the SLR indicates that the effective refractive index for this mode increases when the YAG:Ce waveguide thickness grows.

To elucidate the fields associated with these modes, we examine the spatial distribution of the intensity of the total electric field for the $d$ = 300 nm sample, where the three modes appear most distinctively. Note that the thickness of the waveguide is slightly larger than the value indicated in Section 2. Figure 6(c) shows the total electric field intenisty enhancement, i.e. total electric field intensity normalized by the incident field intensity, at $\lambda$ = 650 nm in the x-z plane at y intersecting the center of the nanorod in a unit cell of the array. At this wavelength, the array supports the LSPRs. The maximum field enhancement is found close to the edges of the silver nanorod and the field in the YAG:Ce layer is negligible, indicating the localized

#179840 - $15.00 USD Received 19 Nov 2012; revised 28 Jan 2013; accepted 28 Jan 2013; published 12 Feb 2013

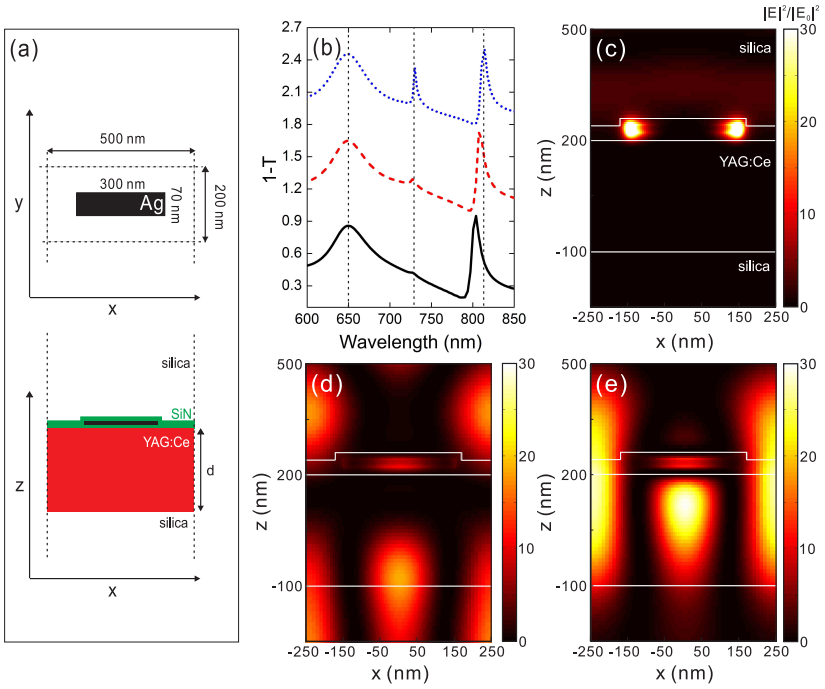


Fig. 6. Simulation using a 3D finite-difference time-domain method. (a) Sketch of the simulated structure. The top panel displays the x-y plane (top view) of the structure. The black square indicates the Ag nanorod, and dotted lines indicate the unit cell of the structure. The bottom panel shows the x-z plane (side view) of the structure. The thickness of the YAG:Ce layer, $d$, was varied from 200 nm to 300 nm. (b) Calculated extinction ($1 - T$) at normal incidence for the structures with $d$ = 200 (black solid curve), 250 (red dashed curve), and 300 nm (blue dotted curve). The curves are vertically shifted by 0.8 from each other for clarity. Dotted vertical lines indicate the wavelengths at which the total electric field intenisty enhancement distribution was calculated for the $d$ = 300 nm structure. (c),(d),(e) The field intenisty distribution in the x-z plane, at y intersecting the middle of the nanorod. The intensity enhancement was calculated for the $d$ = 300 nm structure using a plane wave with wavelength of 650 nm (b), 730 nm (c), and 814 nm (c) illuminating the unit cell of the array at normal incidence. The interfaces between silica/$Si_3N_4$, $Si_3N_4$/YAG:Ce, and YAG:Ce/silica are highlighted by white lines.

#179840 - $15.00 USD Received 19 Nov 2012; revised 28 Jan 2013; accepted 28 Jan 2013; published 12 Feb 2013

nature of the LSPRs. Figures 6(d) and 6(e) show the field distribution at $\lambda$ = 730 and 814 nm, corresponding to the quasi-guided modes and the SLR, respectively. In these plots, the field is distributed both around the nanorod and in the YAG:Ce layer, showing the hybridized nature of these modes with the LSPRs. The large field intensity inside the layer suggests that the excited YAG:Ce can efficiently decay into these modes, which can couple out into free space radiation in defined directions. This behaviour qualitatively explains the large PL enhancement observed at the wavelengths of the quasi-guided mode and the SLR in a direction normal to the surface. Compared to the quasi-guided mode, the field intensity is more confined in the plane of the nanorod array in the case of the SLR, because it originates from the diffraction in the plane of the array. The intensity in the YAG:Ce layer is stronger in Fig. 6(e) than in 6(d), which is in agreement with the experimental results displayed in Fig. 5 where the strongest enhancement was achieved for the SLR.

## 6. Conclusions

We have examined the conditions for the excitation of hybrid plasmonic-photonic modes in arrays of plasmonic particles coupled to light-emitting waveguides. Depending on the refractive index of the media surrounding the array, the samples can sustain surface lattice resonances and/or quasi-guided modes. We have found for the first time that both modes can be excited simultaneously when the refractive index of the upper medium of the array is similar to that of the lower medium. By making use of the optical emitters in the waveguide as local probes, we have investigated the coupling of light emission to these hybrid modes. Light emission shows a strong spectral modification and a noteworthy increase in intensity at the angles and wavelengths that correspond to those modes. The increased LDOS and enhanced outcoupling are responsible for this increased emission. It is worth pointing out that having both surface lattice resonances and quasi-guided modes are beneficial for light management techniques not only in the fields of solid state lighting but also for thin films solar cells [46] and sensors [47].

## Acknowledgments

This work is part of the research programme of the Foundation for Fundamental Research on Matter (FOM), which is financially supported by the Netherlands Organization for Fundamental Research (NWO), and it is part of an industrial partnership program between Philips and FOM. This work is also supported by NanoNextNL, a micro and nanotechnology consortium of the Government of the Netherlands and 130 partners. S.M. is grateful for Young Researcher Overseas Visits Program for Vitalizing Brain Circulation of JSPS, and Grant-in-Aid for Scientific Research (C, No. 24560824) from MEXT, Japan.

#179840 - $15.00 USD Received 19 Nov 2012; revised 28 Jan 2013; accepted 28 Jan 2013; published 12 Feb 2013